Magneto-dielectric, optical and electrical behavior of $Zn_{0.5}Co_{0.25}Cu_{0.25}Re_{0.125}Fe_{1.875}O_4$ (Re = La^{3+} and Ce^{3+}) spinel ferrites

K. Mehmood [a], R. Alabada [b], M. I. Arshad [a], N. Ali [a], N. Amin [a], Enam-ul- Haq [a], M. S. Al-Buriahi [c], S. F. Mahmoud [d], S. Mumtaz [e], A. U. Rehman [a,*]

[a] *Magnetic & Innovative Materials in Nanotechnology (MIMI Nanotech) Research Lab, Physics Department, Government College University Faisalabad, P.O. Box 38000 Punjab, Pakistan.*

[b]*Al-Muthanna University, College of Pharmacy, Muthanna State, Samawah 66001, Iraq*

[c]*Department of Physics, Sakarya University, Sakarya, Turkey*

[d]*Department of Biotechnology, College of Science, Taif University, Taif city, Saudi Arabia*

[e]*Electrical and Biological Physics, Kwangwoon University, Seoul 01897, South Korea*

In this study, we investigate the structural, optical, and electrical properties of $Zn_{0.5}Co_{0.25}Cu_{0.25}Fe_2O_4$ (ZCCF) spinel ferrites (SFs) and its La^{3+}- and Ce^{3+}-substituted counterparts (ZCCLF and ZCCCF) SFs, synthesized using the sol-gel auto combustion method. The primary focus is on analyzing the temperature-dependent resistivity behavior of these SFs. All samples exhibit semiconducting behavior, with resistivity decreasing as temperature increases from 400 K to 650 K. Undoped ZCCF shows the lowest resistivity, while doping with La^{3+} and Ce^{3+} significantly increases resistivity due to disruptions in charge carrier mobility caused by lattice distortions. Ce^{3+}-doped ZCCCF exhibits the highest resistivity at all temperatures, highlighting the stronger influence of Ce^{3+} compared to La^{3+} on the ferrite's electrical properties. The magnetic properties of ZCCF, ZCCLF, and ZCCCF were analyzed, revealing distinct behaviors. ZCCF exhibited the highest saturation magnetization (68.68 emu/g) and resonance frequency (15.18 GHz), making it suitable for high-frequency applications. ZCCLF showed the highest coercivity (934.18 Oe) and anisotropy, ideal for permanent magnets, while ZCCCF displayed the lowest coercivity (46.43 Oe), indicating soft magnetic characteristics for easy magnetization switching.

(Received February 5, 2025; Accepted June 10, 2025)

Keywords: Spinel, Auto combustion, Structural, Optical, Electrical, Magnetic

1. Introduction

Spinel ferrites (SFs) stand out amongst the most vital and attractive magnetic materials which is why they are widely utilized nowadays in electronic innovations. In the most recent couple of decades, researchers inquired that uncovers that SFs of mixed character are superior magnetic supplies than metals not mixed with other metals due to their cost effectiveness, improved efficiency, and novel structural, optical, and electrical properties, because of these characteristics SFs have huge applications in the field of technology like low magnetized ferrofluids, sensors and in drugs delivery as magnetic carriers [1, 2].

SFs have the general equation of AB_2O_4, A, and B are metallic cations situated at different diverse crystallographic destinations, A is at the tetrahedral site, B is the octahedral site, and Fe (III) is one of the constituents in their structure. Depending upon the arrangement of the M (divalent) and Fe (trivalent) positions, there are three kinds of SFs classes known, normal, mixed, and inverse. When M (divalent) is situated at the tetrahedral site this type of structure is called normal spinel while Fe (trivalent) is present at the octahedral site. In inverse ferrite spinel structure, Fe(III) located at the two different sites half of Fe atoms occupy tetrahedral or A-sites, and the remaining half

* Corresponding author: attaurrehman423@gmail.com
https://doi.org/10.15251/JOR.2025.213.343

together with M (II) occupy octahedral or B-sites, while M (II) occupies B sites. In mixed spinel structure ferrite, both particles arbitrarily possess the tetrahedral and octahedral destinations [3, 4].

Different techniques [5, 6] are present to prepare SFs including the sol-gel auto-combustion method, co-precipitation technique, hydrothermal method, and microemulsion. Co-precipitation offers a simple, cost-effective method for synthesizing homogeneous materials, particularly useful in nanotechnology and catalysis. It ensures uniform mixing of components and allows control over particle size by adjusting factors like pH and temperature. The process is scalable, making it ideal for both laboratory and industrial applications [7].

The novelty of this work lies in the synthesis and characterization of $Zn_{0.5}Co_{0.25}Cu_{0.}25Re_{0.125}Fe_{1.875}O_4$ (Re = La^{3+} and Ce^{3+}) SFs using the SGAC method, which introduces a unique multi-element doping approach in the spinel ferrite structure. By incorporating both transition metals (Zn, Co, Cu) and rare-earth elements (La^{3+}, Ce^{3+}), the study aims to investigate how these diverse dopants influence the material's structural, optical, and electrical properties. This specific combination of dopants is relatively unexplored, and the research potentially uncovers new insights into tailoring ferrite properties for advanced applications, such as in electronic devices, sensors, or magnetic materials. Additionally, the use of co-precipitation offers a simple, scalable synthesis route with better control over homogeneity and particle size, contributing to the novelty. The study's focus on rare-earth substitution and its impact on dielectric and optical behaviors further enhances its uniqueness, providing a comprehensive understanding of the interplay between composition and functional properties.

2. Experimental part

The sol-gel auto-combustion method for preparing $Zn_{0.5}Co_{0.25}Cu_{0.25}Re_{0.125}Fe_{1.875}O_4$ (Re = La^{3+} and Ce^{3+}) involves dissolving stoichiometric amounts of metal nitrates $Zn(NO_3)_2.6H_2O$, $Cu(NO_3)_2.6H_2O$, $Co(NO_3)_2.3H_2O$, $Fe(NO_3)_3.9H_2O$, $La(NO_3)_3.6H_2O$ and $Ce(NO_3)_3.6H_2O$ in deionized water, followed by the addition of citric acid as a chelating agent in a 1:1 molar ratio with total metal ions. The pH is adjusted to 7–8 using an ammonia solution, and the mixture is heated at 80–100 °C to form a viscous gel. Upon transferring the gel to a furnace at 200–250°C, it undergoes auto-combustion, producing a voluminous ash-like powder. The resulting product is calcined at 600–800°C for 2–4 hours to remove residual organic matter and enhance crystallinity. The chemical reactions are given below:

$$\text{Metal Nitrates} + \text{Citric Acid} + NH_3 \xrightarrow{\text{Combustion}} Zn_{0.5}Co_{0.25}Cu_{0.25}Re_{0.125}Fe_{1.875}O_4 + \text{Gaseous Byproducts}$$

3. Results and discussion

3.1. Phase and structural analysis

To examine the phase purity and lattice parameters XRD characterization process was used [8]. Fig. 1 shows diffraction peaks appear at 30.02°, 35.35°, 46.95°, and 57.51° the planes of peaks (220), (311), (222), (400), (331), (422), and (511) respectively, and verified the development of single phase. The d-spacing (d) of as-prepared SFs was calculated using Bragg's law [9];

$$d = \frac{n\lambda}{2\sin\theta} \quad (1)$$

where n = 1, λ is the wavelength of the X-ray used. The lattice constant (a) was estimated via relation [10];

$$a = d_{hkl}\sqrt[2]{[h^2 + k^2 + l^2]} \quad (2)$$

The crystallite size (D) was estimated by Scherrer's equation [5]:

$$D = \frac{K\,\lambda}{\beta\,cos\theta} \tag{3}$$

where k constant is taken as 0.98, β is the full-width half maximum (FWHM) of the peak and θ angle of diffraction. The X-ray density (ρ_X) was determined using the equation [11];

$$\rho_X = \frac{ZM}{N_A\,a^3} \tag{4}$$

Table 1 shows that the lattice constant was decreased with increasing rare earth ions La^{3+} and Ce^{3+} in the ZCCF lattice. It may be due to the replacement of larger ionic radii La^{3+} and Ce^{3+} ions by Fe^{3+} ions. The X-ray density was also reduced with the doping of La^{3+} and Ce^{3+} ions. It was also seen that crystalline size was reduced from 30.16 nm to 17.83 nm. It may be due to strong Re^{3+} $–O^{2-}$ bond as compared to Fe^{3+}–O^{2-} bond.

Table 1. Structural parameters for all the samples.

Compositions	d-spacing (Å)	Lattice constant (Å)	Crystallite Size (nm)	X-Ray Density (g/cm^3)	Energy bandgap (eV)
$Zn_{0.5}Co_{0.25}Cu_{0.25}Fe_2O_4$ (ZCCF)	2.654	8.406	30.16	5.869	4.00
$Zn_{0.5}Co_{0.25}Cu_{0.25}La_{0.125}Fe_{1.875}O_4$ (ZCCLF)	2.542	8.402	24.48	5.872	3.84
$Zn_{0.5}Co_{0.25}Cu_{0.25}Ce_{0.125}Fe_{1.875}O_4$ (ZCCCF)	2.487	8.353	17.83	5.960	3.62

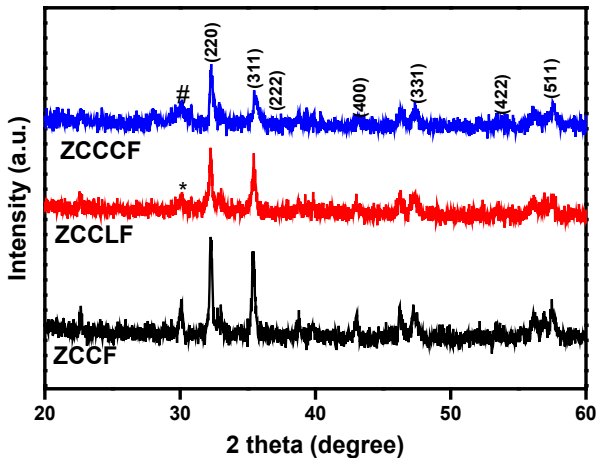

Fig. 1. XRD pattern for ZCCF, ZCCLF, and ZCCCF samples.

3.2. UV-vis analysis

The coefficient of absorption (α) was calculated by using the following equation [12];

$$\alpha = 2.303 \log A/\,t,$$

where "t" is the sample's thickness and "A" is the absorbance. Tauc's relation [13] was used to show the relation between energy bandgap (E_g) and coefficient of absorbance (α).

$$\alpha h\nu = B(h\nu - E_g)^m$$

where “m” is a constant that depends on the nature of the transition between the valence and conduction band. The “hν” is the energy of the incident photon and B is constant. The value of m for the direct band is ½ while for the indirect band is 2. It was observed that with the substitution of La^{3+} and Ce^{3+} ions in the ZCCF sample, the energy bandgap was reduced from 4.00 eV to 3.60 eV (as shown in Table 1).

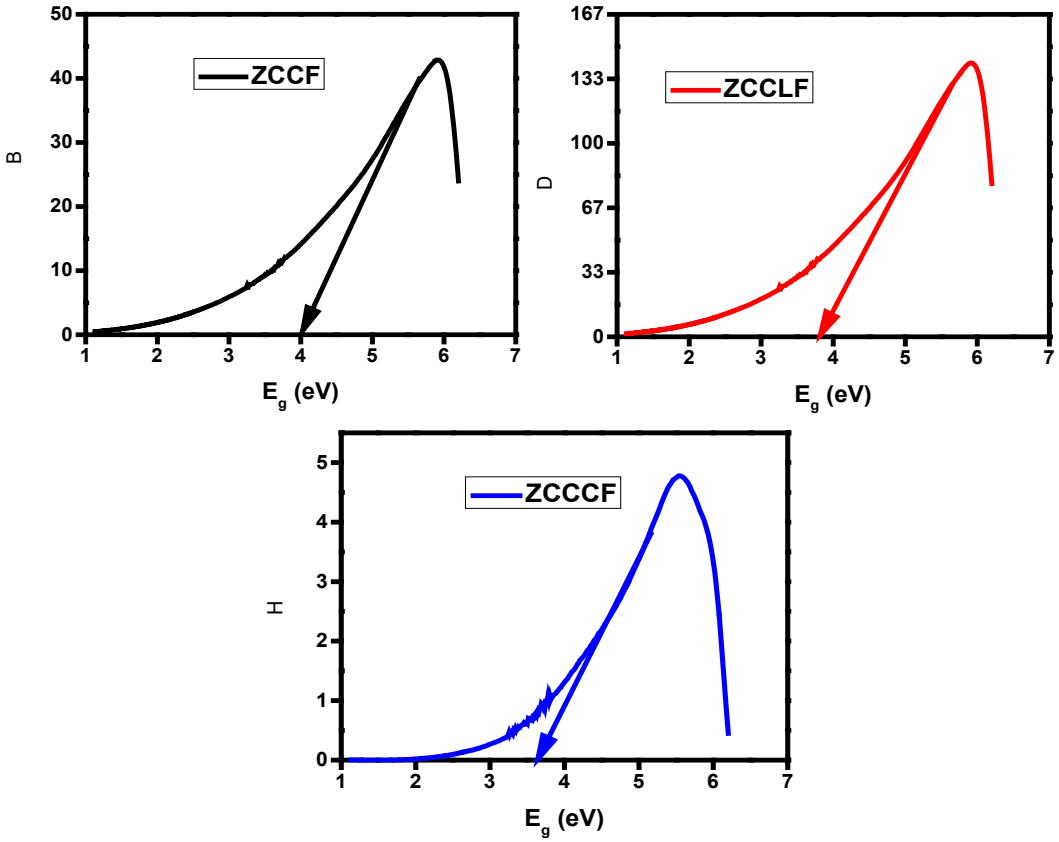

Fig. 2. Tauc plots for ZCCF, ZCCLF, and ZCCCF samples.

3.3. Electrical analysis

Table 2 provides resistivity (ρ) values for three different SFs samples including ZCCF, ZCCLF, and ZCCCF SFs at temperatures ranging from 400 K to 650 K, illustrating how rare-earth doping (La^{3+} and Ce^{3+}) influences the resistivity behavior compared to the undoped ferrite (ZCCF). All three compositions display a characteristic semiconducting behavior, where resistivity decreases with increasing temperature, due to enhanced thermal excitation of charge carriers, typical of ferrite materials [14, 15]. Among the compositions, the undoped ferrite (ZCCF) has the lowest resistivity across all temperatures, starting at 5.3701 × 10^7 Ω cm at 400 K and decreasing sharply to 0.0026 × 10^7 Ω cm at 650 K. This significant drop suggests that ZCCF has a relatively high conductivity compared to the doped samples.

Doping with La^{3+} (ZCCLF) increases the resistivity significantly compared to ZCCF. At 400 K, ZCCLF has a resistivity of 22.0062 × 10^7 Ω cm, which is about four times higher than ZCCF at the same temperature. However, it still exhibits a decrease in resistivity with rising temperature, dropping to 0.0238 × 10^7 Ω cm at 650 K. The increased resistivity due to La^{3+} doping can be attributed to the introduction of La^{3+} ions, which disrupts the hopping mechanism between Fe^{2+} and Fe^{3+} ions in the ferrite structure, thereby reducing charge carrier mobility [16].

Ce^{3+} doping (ZCCCF) results in an even more pronounced increase in resistivity, with the highest values among the three samples. At 400 K, ZCCCF has a resistivity of 67.7079 × 10^7 Ω cm, which is nearly 13 times higher than that of ZCCF. Even though its resistivity decreases as

temperature increases, the value at 650 K remains relatively high at 0.4345 × 10^7 Ω cm, compared to the other samples. This large increase in resistivity due to Ce^{3+} doping can be attributed to the larger ionic radius of Ce^{3+} compared to Fe^{3+}, which distorts the ferrite lattice more significantly than La^{3+}, further hindering the charge transfer process. Both rare-earth dopants (La^{3+} and Ce^{3+}) introduce additional lattice defects and local distortions that interfere with electron hopping, leading to increased resistivity [17].

Overall, Table 2 demonstrates that rare-earth doping (La^{3+} and Ce^{3+}) significantly influences the resistivity behavior of ZnCoCu SFs, with Ce^{3+} showing a more pronounced effect than La^{3+} (as shown in Fig. 3(a-c)). The variation in resistivity with temperature and composition provides valuable insights into the tuning of electrical properties in ferrite materials through rare-earth ion substitution, which can be advantageous for specific applications in electronics and magnetic devices where controlled resistivity is crucial [18-21].

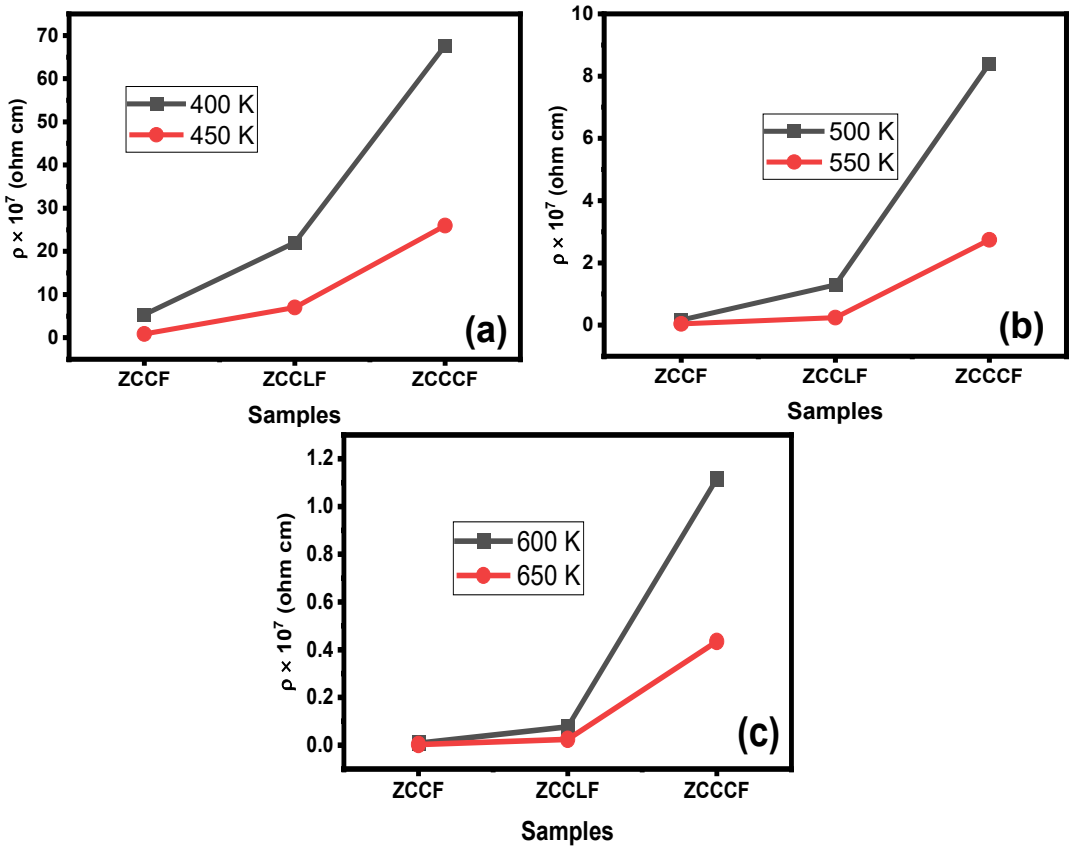

Fig. 3. (a-c) Resistivity vs. samples at different temperatures for ZCCF, ZCCLF, and ZCCCF samples.

Table 2. Values of resistivity (ρ) of ZCCF, ZCCLF, and ZCCCF samples at different temperature.

Composition	Resistivity ρ × 10^7 (Ω cm)					
	400 K	450 K	500 K	550 K	600 K	650 K
$Zn_{0.5}Co_{0.25}Cu_{0.25}Fe_2O_4$ (ZCCF)	5.3701	0.8605	0.1597	0.0394	0.0082	0.0026
$Zn_{0.5}Co_{0.25}Cu_{0.25}La_{0.125}Fe_{1.875}O_4$ (ZCCLF)	22.0062	6.9814	1.2917	0.2378	0.0771	0.0238
$Zn_{0.5}Co_{0.25}Cu_{0.25}Ce_{0.125}Fe_{1.875}O_4$ (ZCCCF)	67.7079	25.9525	8.4068	2.7416	1.1169	0.4345

3.4. Dielectric analysis

The dielectric constant represents the material's ability to store electrical energy. In spinel ferrites, the dielectric constant is high at low frequencies but decreases as the frequency increases. Fig. 4(a) shows the variation of the dielectric constant with frequency and samples. This behavior is due to dielectric dispersion, a phenomenon where the polarization mechanisms fail to keep up with the alternating electric field at higher frequencies. At low frequencies: The dominant contribution comes from space charge polarization, caused by the migration of charge carriers (e.g., $Fe^{2+} \leftrightarrow Fe^{3+}$ hopping at octahedral sites). These carriers can follow the slowly varying electric field, resulting in a high dielectric constant. At high frequencies: The electric field changes rapidly, and the dipoles (or charge carriers) cannot realign themselves fast enough. This reduces the polarization and, consequently, the dielectric constant. Among the samples, ZCCF shows the highest dielectric constant at low frequencies. This could be attributed to its specific composition and microstructure, such as grain size and cation distribution, which enhance the mobility of charge carriers at octahedral sites.

Dielectric loss indicates the energy dissipated as heat during polarization. Similar to the dielectric constant, dielectric loss is higher at low frequencies and decreases with increasing frequency (as shown in Fig. 4(b)). At low frequencies: The energy dissipation is significant due to charge hopping between Fe^{2+} and Fe^{3+} ions, as well as ionic displacement. Additionally, defects or impurities in the material contribute to higher losses. At high frequencies: The hopping process becomes less effective because the alternating electric field changes too quickly for the ions to respond. As a result, the energy dissipation (dielectric loss) reduces. ZCCF shows the highest dielectric loss at low frequencies, possibly due to more charge carrier hopping or higher defect density in its structure compared to ZCCLF and ZCCCF.

AC conductivity (σ_{AC}) measures the material's ability to conduct an alternating current. In spinel ferrites, AC conductivity increases with frequency, a behavior consistent with universal dielectric response (Fig. 4(c)). At low frequencies: The AC conductivity is low because the hopping of charge carriers (such as $Fe^{2+} \leftrightarrow Fe^{3+}$) is limited. The conduction occurs predominantly through localized charge carriers. At high frequencies: The alternating electric field facilitates more frequent hopping of charge carriers between cation sites, leading to increased conductivity. This is often attributed to the small polaron hopping mechanism in ferrites. The ZCCLF and ZCCCF samples show higher AC conductivity than ZCCF, likely due to differences in grain boundaries, cation distribution, or improved charge carrier mobility. Grain size plays a critical role smaller grains lead to more grain boundaries, which can trap charge carriers and lower conductivity.

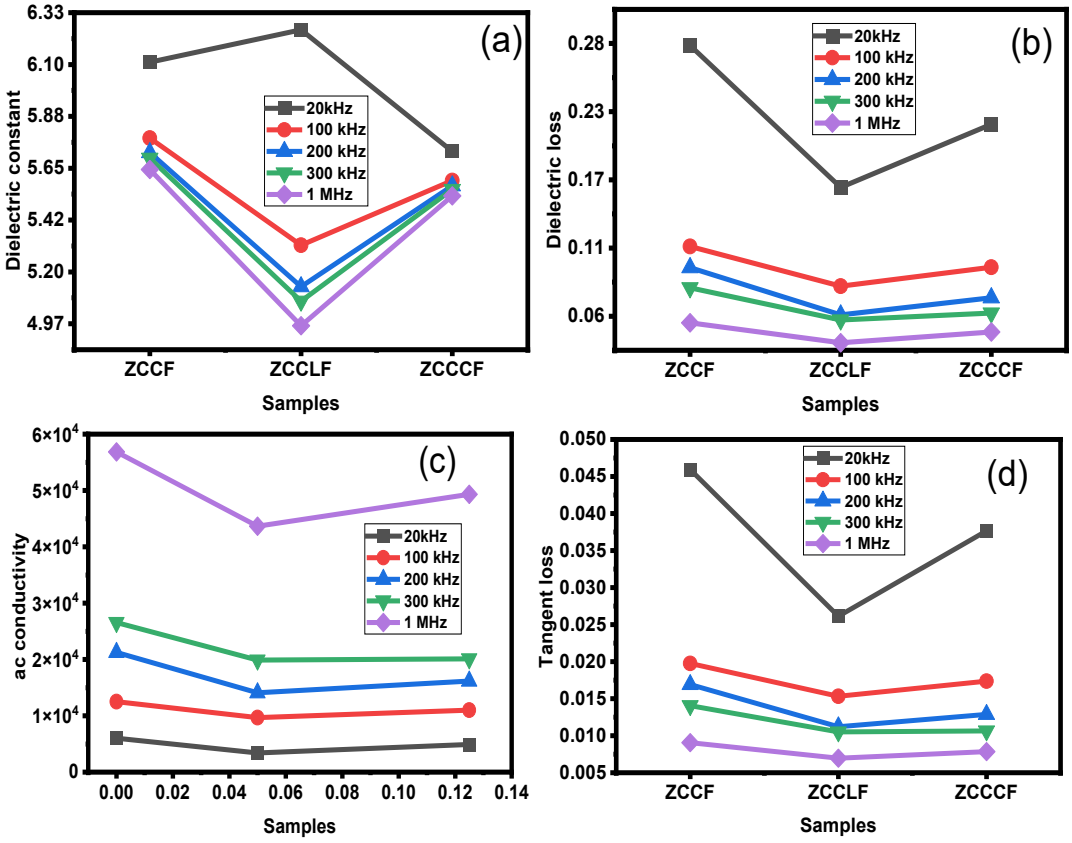

Fig. 4. (a-d) Dielectric parameters for ZCCF, ZCCLF, and ZCCCF samples.

Tangent loss (tan δ) represents the ratio of the energy dissipated as heat to the energy stored in the material. Similar to dielectric loss, tangent loss decreases with increasing frequency (as depicted in Fig. 4(d)). At low frequencies: The energy dissipation is higher because charge carriers can follow the alternating field, leading to significant polarization and loss. At high frequencies: The inability of charge carriers to keep up with the fast-changing electric field reduces energy dissipation, resulting in lower tangent loss. The ZCCF sample shows higher tangent loss at low frequencies, reflecting greater energy dissipation, possibly due to higher defect density or more prominent hopping mechanisms in its microstructure. ZCCLF and ZCCCF exhibit lower tangent loss, suggesting more stable and less loss structures at these frequencies.

3.5. Magnetic analysis

The magnetization (M) *vs.* applied field (H) plots in Fig. 5 revealed hysteresis loops for ZCCF, ZCCLF, and ZCCCF samples. The plots suggest a relatively softer magnetic nature with lower coercivity. Table 2 contains magnetic parameters: saturation magnetization (Ms), remanent magnetization (Mr), coercivity (Hc), squareness ratio (SQ), anisotropy constant (K), and microwave operating frequency (ω_m). A higher Ms indicates a stronger magnetic response, meaning more magnetic moments per unit mass align in the applied field. ZCCF (68.68 emu/g) has the highest Ms, meaning it has the most magnetic moments available for alignment, likely due to higher Fe content or a more ferromagnetic phase [22]. ZCCLF (55.35 emu/g) and ZCCCF (49.51 emu/g) have lower Ms, suggesting either a weaker magnetic phase or the presence of non-magnetic impurities [15].

A higher M_r means the material retains more magnetization even after the field is removed. ZCCLF has the highest M_r (26.13 emu/g), indicating that it is closer to a hard magnetic material, were magnetic domains resist realignment. ZCCCF has the lowest M_r (3.73 emu/g), meaning it loses magnetization quickly, making it suitable for soft magnetic applications [23]. ZCCF (9.43 emu/g) lies in between, showing moderate retention of magnetization.

A higher H_c indicates a hard magnetic material. A lower H_C means a soft magnetic material. ZCCLF has the highest Hc (934.18 Oe), indicating it is highly resistant to demagnetization, making it suitable for permanent magnet applications. ZCCCF has the lowest HcH_cHc (46.43 Oe), meaning it is easily magnetized and demagnetized, useful for transformer cores and electromagnetic applications. ZCCF (113.95 Oe) has moderate Hc, suggesting a balance between soft and hard magnetic properties [24]. ZCCLF has the highest SQ (0.4720), meaning it has strong magnetic retention (good for hard magnets). ZCCCF has the lowest SQ (0.0753), suggesting it quickly loses magnetization, ideal for soft magnetic applications. ZCCF (0.1373) lies between the two, meaning it retains some magnetization but is still relatively easy to demagnetize [25]. Higher K means stronger anisotropy, meaning more energy is needed to change the magnetic state. ZCCLF has the highest K (53861.32 erg/cm³), meaning it strongly prefers a particular magnetization direction, making it ideal for permanent magnets. ZCCCF has the lowest K (2394.53 erg/cm³), meaning it can easily change magnetization direction, useful for soft magnetic applications. ZCCF (8152.17 erg/cm³) has moderate anisotropy, indicating some stability but still allowing for relatively easy realignment [26].

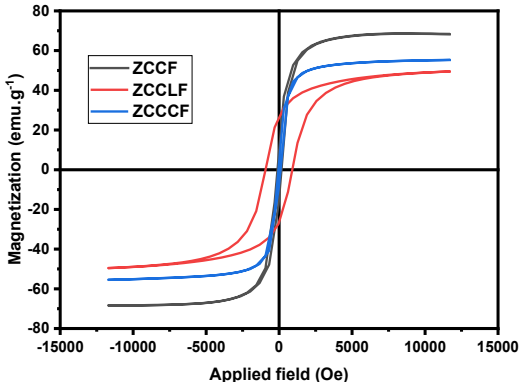

Fig. 5. MS loops for ZCCF, ZCCLF, and ZCCCF samples.

Table 3. Magnetic properties of as-prepared samples.

Samples	M_S (emu.g^{-1})	M_r (emu.g^{-1})	H_C (Oe)	SQ ratio	K (erg. cm^{-3})	ω_m (GHz)
ZCCF	68.68	9.43	113.95	0.1373	8152.17	15.18
ZCCLF	55.35	26.13	934.18	0.4720	53861.32	12.23
ZCCCF	49.51	3.73	46.43	0.0753	2394.53	10.94

A higher ω_m means the material can operate at higher frequencies before losing efficiency. ZCCF has the highest ω_m (15.18 GHz), ZCCLF (12.23 GHz), and ZCCCF (10.94 GHz) making it ideal for high-frequency magnetic devices [3].

4. Conclusions

The $Zn_{0.5}Co_{0.25}Cu_{0.}25Re_{0.125}Fe_{1.875}O_4$ (Re = La^{3+} and Ce^{3+}) SFs were prepared using the co-precipitation method. The lattice constant and energy bandgap were reduced with the addition of La^{3+} and Ce^{3+} ions in ZCCF SFs. Moreover, the study concludes that ZCCF SFs exhibit typical semiconducting behavior, with resistivity decreasing as temperature rises from 400 K to 650 K. Rare-earth doping with La^{3+} and Ce^{3+} significantly increases the resistivity compared to the undoped ferrite, as these ions disrupt the charge carrier mobility by interfering with the electron hopping

mechanism between Fe^{2+} and Fe^{3+}. Ce^{3+}-doped ferrite (ZCCCF) shows the highest resistivity, indicating that Ce^{3+} has a stronger impact on the ferrite structure than La^{3+}. This suggests that Ce^{3+} creates more pronounced lattice distortions, which further hinder conductivity. ZCCF is best for high-magnetization applications, ZCCLF is ideal for hard magnetic uses (high Hc and K), and ZCCCF is better for applications requiring low coercivity and easy re-magnetization. The ability to tune the electrical properties through rare-earth substitution makes these ferrites suitable for applications in electronic devices and sensors where controlled resistivity is important.

Acknowledgments

The authors extend their appreciation to Taif University, Saudi Arabia, for supporting this work through project number (TU-DSPP-2024-53).

Declaration of competing interest

The authors declare that they have no known competing financial interests or personal relationships that could have appeared to influence the work reported in this paper.

Data availability

Data will be made available on request.

References

[1] K. Gayakvad, K. Somdatta, V. Mathe, T. Dongale, K. Patankar, Emergent Materials, 7 (2024) 103-131; https://doi.org/10.1007/s42247-023-00576-y

[2] M. Fatima, M.S.U. Hasan, M. Akhtar, N. Morley, N. Amin, A.u. Rehman, M.I. Arshad, M. Amami, B. Yaqub, S. Ezzine, ACS omega, 8 (2023) 41169-41181; https://doi.org/10.1021/acsomega.3c03993

[3] A.U. Rehman, G. Abbas, B. Ayoub, N. Amin, M.A. un Nabi, N.A. Morley, M. Akhtar, M.I. Arshad, M.U. Khalid, M. Afzaal, Materials Science and Engineering: B, 291 (2023) 116407; https://doi.org/10.1016/j.mseb.2023.116407

[4] X. Ren, G. Xu, Journal of magnetism and magnetic materials, 354 (2014) 44-48; https://doi.org/10.1016/j.jmmm.2013.10.056

[5] A.U. Rehman, S. Sharif, H. Hegazy, N. Morley, N. Amin, M. Akhtar, M.I. Arshad, Z. Farooq, Z. Munir, T. Munir, Materials Today Communications, (2023) 105371; https://doi.org/10.1016/j.mtcomm.2023.105371

[6] A.U. Rehman, N. Morley, N. Amin, M.I. Arshad, M.A. un Nabi, K. Mahmood, A. Ali, A. Aslam, A. Bibi, M.Z. Iqbal, Ceramics International, 46 (2020) 29297-29308; https://doi.org/10.1016/j.ceramint.2020.08.106

[7] K. Hussain, A. Bibi, F. Jabeen, N. Amin, K. Mahmood, A. Ali, M.Z. Iqbal, M. Arshad, Physica B: Condensed Matter, 584 (2020) 412078; https://doi.org/10.1016/j.physb.2020.412078

[8] M. Huq, D. Saha, R. Ahmed, Z. Mahmood, Journal of Scientific Research, 5 (2013) 215-234; https://doi.org/10.3329/jsr.v5i2.12434

[9] M.A. Iqbal, M. Islam, I. Ali, I. Sadiq, I. Ali, Journal of alloys and compounds, 586 (2014) 404-410; https://doi.org/10.1016/j.jallcom.2013.10.066

[10] M. Ishaque, M.A. Khan, I. Ali, M. Athair, H.M. Khan, M.A. Iqbal, M. Islam, M.F. Warsi, Materials Science in Semiconductor Processing, 41 (2016) 508-512; https://doi.org/10.1016/j.mssp.2015.10.028

[11] A. Aslam, A.U. Rehman, N. Amin, M.A. un Nabi, Q. ul ain Abdullah, N. Morley, M.I. Arshad, H.T. Ali, M. Yusuf, Z. Latif, Journal of Physics and Chemistry of Solids, 154 (2021) 110080; https://doi.org/10.1016/j.jpcs.2021.110080

[12] N.-u.-H. Khan, Z.A. Gilani, G. Hussain, M. Khalid, H. Asghar, M.A. Shar, S.M. Ali, M.A. Khan, F.A. Sheikh, Indian Journal of Physics, (2024) 1-18; https://doi.org/10.1007/s12648-024-03137-z

[13] A. Aslam, A.U. Rehman, N. Amin, M. Amami, M.A.u. Nabi, H. Alrobei, M. Asghar, N. Morley, M. Akhtar, M.I. Arshad, Journal of Superconductivity and Novel Magnetism, (2022) 1-11; https://doi.org/10.1007/s10948-021-06085-5

[14] G. Abbas, A.U. Rehman, W. Gull, M. Afzaal, N. Amin, L. Ben Farhat, M. Amami, N.A. Morley, M. Akhtar, M.I. Arshad, Journal of Sol-Gel Science and Technology, 101 (2022) 428-442; https://doi.org/10.1007/s10971-021-05713-9

[15] M. Akhtar, A.U. Rehman, N. Amin, K. Hussain, M.I. Arshad, Journal of Magnetism and Magnetic Materials, (2024) 171831; https://doi.org/10.1016/j.jmmm.2024.171831

[16] M. Akram, S. Akhlaq, M.I. Arshad, N. Amin, A.A. Ifseisi, M. Akhtar, N.T.K. Thanh, N. Morley, S. Sadiq, S. Hussain, Solid State Communications, 373 (2023) 115317; https://doi.org/10.1016/j.ssc.2023.115317

[17] M.I. Arshad, M. Hasan, A.U. Rehman, M. Akhtar, N. Amin, K. Mahmood, A. Ali, T. Trakoolwilaiwan, N.T.K. Thanh, Ceramics International, 48 (2022) 14246-14260; https://doi.org/10.1016/j.ceramint.2022.01.313

[18] M.I. Arshad, K. Mehmood, N. Amin, N. Morley, N.T.K. Thanh, Composites Communications, 39 (2023) 101571; https://doi.org/10.1016/j.coco.2023.101571

[19] S. Arshad, M.I. Arshad, A.U. Rehman, N. Amin, M. Ajaz-un-Nabi, Materials Science and Engineering: B, 299 (2024) 117019; https://doi.org/10.1016/j.mseb.2023.117019

[20] A. Aslam, A. Razzaq, S. Naz, N. Amin, M.I. Arshad, M.A.U. Nabi, A. Nawaz, K. Mahmood, A. Bibi, F. Iqbal, Journal of Superconductivity and Novel Magnetism, (2021) 1-10; https://doi.org/10.1007/s10948-021-05802-4

[21] E.E. Ateia, M. Ahmed, L. Salah, A. El-Gamal, Physica B: Condensed Matter, 445 (2014) 60-67; https://doi.org/10.1016/j.physb.2014.03.094

[22] M.F. Abou Taleb, M.M. Ibrahim, A. Rahman, Z.M. El-Bahy, Ceramics International, 50 (2024) 37077-37084; https://doi.org/10.1016/j.ceramint.2024.07.096

[23] S.M. Suryawanshi, K.V. Chandekar, D.S. Badwaik, V.V. Warhate, N.M. Gahane, S.R. Daf, Inorganic Chemistry Communications, 156 (2023) 111204; https://doi.org/10.1016/j.inoche.2023.111204

[24] M. Sikder, M. Hossain, I. Sardar, M.S. Hossain, M. Khan, M. Rahman, Results in Physics, 46 (2023) 106320; https://doi.org/10.1016/j.rinp.2023.106320

[25] M. Roy-Chowdhury, S.K. Jena, V.P. Khadse, D.C. Joshi, S. Thota, Journal of Physics D: Applied Physics, 56 (2023) 355304; https://doi.org/10.1088/1361-6463/acd5dd

[26] R. Ranga, K. Kumar, A. Kumar, Journal of Magnetism and Magnetic Materials, 588 (2023) 171496; https://doi.org/10.1016/j.jmmm.2023.171496